Adsorptive removal of p-nitrophenol from water with mechano-synthesized porous organic polymers

Journal:	*New Journal of Chemistry*
Manuscript ID	NJ-ART-09-2018-004575.R1
Article Type:	Paper
Date Submitted by the Author:	21-Oct-2018
Complete List of Authors:	Zeng, Heng; Jinan University Lu, Weigang; Jinan University, Hao, Leiduan; Washington State University, Chemistry Helms, Gregory; Washington State University, Center for NMR Spectroscopy ZHANG, QIANG; Washington State University, Chemistry Luo, Zhiping; Fayetteville State University, Chemistry and Physics

Journal Name

ARTICLE

Adsorptive removal of p-nitrophenol from water with mechano-synthesized porous organic polymers

Received 00th January 20xx,
Accepted 00th January 20xx

DOI: 10.1039/x0xx00000x

www.rsc.org/

Heng Zeng,[a] Weigang Lu,*[a,c] Leiduan Hao,[b] Gregory L. Helms[b], Qiang Zhang*[b] and Zhiping Luo[c]

In this work, we demonstrated a successful synthesis of porous organic polymers *via* a ball-milling procedure. Several readily available benzene derivatives were selected to be polymerized through a Friedel-Crafts reaction with $FeCl_3$ as Lewis acid catalyst and formaldehyde dimethyl acetal as a crosslinker. All the mechano-synthesized porous organic polymers (MPOPs) are not soluble in common organic solvents, and the calculated surface area was over 500 m^2/g when biphenyl was used as the monomer. One of the advantages of applying ball-milling in targeted polymer synthesis is bypassing the large quantity of hazardous chlorinated solvents which are commonly used in traditional Friedel-Crafts reactions. Considering the aromatic skeleton and hydrophobic nature of these polymers, their performances in p-nitrophenol (PNP) adsorption from water was investigated. The quantification was carried out on an Ionic 3Q 320 LC-MS/MS system with 4-nitrocatechol (PNC) as an internal standard. MPOP-1 and MPOP-3 showed maximum adsorption capacity of 133.10 and 155.51 mg/g for PNP, respectively. The adsorption kinetics were studied and both adsorption isotherms were well delineated with a pseudo-second-order equation, indicating the availability of strong adsorption sites in both MPOPs for interacting with PNP.

Introduction

Porous organic polymers (POPs),[1] along with metal-organic frameworks (MOFs),[2] have recently been identified to have potential in storage and separation of small molecules due to their exceptionally high porosity and tunable functionality. POPs are porous materials comprised of light, non-metallic elements such as carbon, hydrogen, boron, oxygen, nitrogen, silicon, and phosphorus that are connected through strong covalent bonds, which render them superior framework stability. As a result, POPs are favorable for post-synthetic modifications to introduce specific chemical functionalities. Indeed, some POPs were handled and derivatized under standard wet chemical reaction conditions without framework degradation or porosity loss.[3]

As a subclass of porous organic polymers, hyper-crosslinked microporous organic polymers (HCPs) are usually generated by transition-metal-catalysed aromatic couplings. They were initially named for the polymeric frameworks synthesized through Friedel-Crafts reactions in the presence of anhydrous $FeCl_3$ as Lewis acid catalyst and formaldehyde dimethyl acetal as a crosslinker,[1g, 4] in which a variety of aromatic derivatives were used as building blocks and polymerized via a $C(sp^2)–C(sp^3)$ cross coupling to produce hyper-crosslinked polymers. They have been thoroughly studied in the fields of gas storage, catalysis, separation and recently carbon capture applications due to their intrinsic porosity and exceptional stability.[4c, 5] Although other Lewis acids and crosslinkers can be used to replace $FeCl_3$ and formaldehyde dimethyl acetal to synthesize HCPs,[6] the Friedel-Crafts coupling process generally requires neither noble metals as catalysts nor the monomers with specific polymerizable groups. Hyper-cross-linking prevents the close packing of polymeric chains in this kind of materials and imparts the frameworks with narrowly dispersed micropores, which lead to decent surface areas and pore volumes.[7]

From a traditional organic synthesis point of view, the preparation of HCPs is of high yield and cost-effective, benefiting from the efficiency of Friedel–Crafts reaction and readily available starting materials.[8] However, chlorinated solvents, such as 1,2-dichloroethane and chloroform, are normally used as reaction media for such syntheses, which is environmentally and economically unsustainable. The growing awareness of the environmental implications of chemical

[a.] *College of Chemistry and Materials Science, Jinan University, Guangzhou, Guangdong, 510632, P.R. China. Email: weiganglu@jnu.edu.cn*
[b.] *Department of Chemistry, Washing State University, Pullman, Washington, 99164, USA. Email: q.zhang@wsu.edu*
[c.] *Research and Technology Transfer Office, Fayetteville State University, Fayetteville, NC 28301, USA.*

Electronic Supplementary Information (ESI) available: additional gas sorption, BET Surface area calculation, UPLC gradient elution, MRM method and parameters for PNP and PNC, pseudo-first-order and pseudo-second-order fittings, SEM images, WDS elemental analysis, Solid-state ^{13}C NMR *etc*. See DOI: 10.1039/x0xx00000x processes and the search for greener solutions have brought untraditional approaches back into the light, especially when it comes to scaling up. To bypass the need for hazardous solvents, mechanochemical synthesis seems to be a promising alternative.[9] The advantages of mechanochemical synthesis of applying ball-milling in targeted polymer synthesis have yet to be explored, where chemical transformations are initiated and sustained by mechanical force.[10] Considering the high yields of mechanochemical reactions along with the easiness to scale up, the prospects of mechano-synthesis are undoubtedly brightening at present and into the future. By utilizing the mechanical energy, ball-milling can be applied not only in many bond-forming processes, including various conventional organic transformations and polymerizations, it can also create stress on substances by different mechanical motions, resulting in nano-sized particles with fine structures that would be otherwise difficult to achieve in solutions, providing opportunities in making new materials desired in certain applications.[11]

In this work, we demonstrated a successful mechano-synthesis of porous organic polymers *via* a ball-milling procedure. Several readily available benzene derivations were selected to be polymerized through a Friedel-Crafts reaction with $FeCl_3$ as Lewis acid catalyst and formaldehyde dimethyl acetal as a crosslinker. Considering the aromatic skeletal structure and hydrophobic nature of these mechano-synthesized porous organic polymers (MPOPs), removal of organic pollutants, especially aromatic ones, from water could be one of the potential applications. Indeed, MPOP-1 and MPOP-3 exhibit maximum absorption capacity of p-nitrophenol (PNP) as high as 133.10 and 155.51 mg/g, respectively. The quantification of PNP in water was carried out on an Ionics 3Q 320 LC-MS/MS system with 4-nitrocatechol (PNC) as an internal standard. Compared with the commonly used UV-Vis spectroscopy, tandem mass spectrometry allows for detection of a low-level concentration with a high degree of specificity and sensitivity. Detection levels using the LC-MS/MS can be as sensitive as several parts per billion.[12]

Experimental

General Information

LC/MS grade acetonitrile, water, methanol, and formic acid were supplied by Fisher Scientific. Other solvents were of ACS grade and used as received. All chemicals including biphenyl, stilbene, tetraphenylethylene, pyrene, naphthalene, toluene, anhydrous $FeCl_3$, Formaldehyde dimethyl acetal (FDA), p-nitrophenol (PNP), and 4-nitrocatechol (PNC) were purchased from Fisher Scientific or VWR International and used as received. Thermalgravimetric (TG) data were obtained on a DTG-60 (SHIMADZU) thermogravimetric analyzer with a heating rate of 5 °C/min under a continuous nitrogen atmosphere. Scanning electron microscopic (SEM) images were collected on JEOL JSM-6510LV Scanning Electron Microscope. Residual iron and chlorine contents were measured by Wavelength-Dispersive X-Ray Spectroscopy on JEOL JXA-8530F Hyperprobe Electron Probe Microanalyzer (EPMA). Adsorption of PNP was quantified on Perkin Elmer Ionics 3Q 320 LC-MS/MS system with PNC as an internal standard. Fourier transform infrared spectroscopy (FT-IR) data were collected on a SHIMADZU IRAffinity-1 Spectrophotometer; the position of an absorption band was given in wavenumbers ν in cm^{-1}. Solid-state ^{13}C NMR investigation was carried out on an Agilent NMR–inova500 with glycine as an external chemical shift reference. The plots are of the TOSS spectra (total suppression of sidebands) which show only the isotropic C-13 peaks.

Synthesis of MPOP-1 to -5 (Scheme 1)

Under a nitrogen atmosphere, formaldehyde dimethyl acetal (0.9 mL, 10.2 mmol) was added to a mixture of anhydrous $FeCl_3$ (2.0 g, 12.3 mmol) and toluene (0.43 mL, 2.2 mmol) in a 65-mL stainless steel grinding vial with two 8-mm steel balls. It was sealed and grounded with 8000M Mixer/Mill for 100 min. 20 mL of aqueous HCl solution (3.0 M) was then added and grounded for another 5 min. The resulting mixture was filtered, the solid was collected and refluxed in a mixture of 20 mL of ethanol/20 mL of aqueous HCl solution (3.0 M) overnight. After cooled down, the solid was collected by filtration, washed with H_2O (3 X 10 mL), ethanol (3 X 10 mL), acetone (3 X 10 mL), and then dried under vacuum at 80 °C for 8 hr to produce MPOP-1 with a yield of 98% (elemental analysis, Fe% 0.178%; Cl% 0.119%).

A similar procedure was followed by using naphthalene (0.27 g, 2.1 mmol) instead to produce MPOP-2 with a yield of 107%, possibly due to the trapped iron and chlorine species (elemental analysis, Fe% 0.622%; Cl% 0.272%).
A similar procedure was followed by using biphenyl (0.32 g, 2.1 mmol) instead to produce MPOP-3 with a yield of 99% (elemental analysis, Fe% 0.786%; Cl% 0.410%).
A similar procedure was followed by using stilbene (0.37 g, 2.1 mmol) instead to produce MPOP-4 with a yield of 115%, possibly due to the trapped iron and chlorine species (elemental analysis, Fe% 0.423%; Cl% 1.078%).

A similar procedure was followed by using tetraphenylethylene (0.34 g, 1.0 mmol) instead to produce MPOP-5 with a yield of 95% (elemental analysis, Fe% 0.799%; Cl% 0.354%).

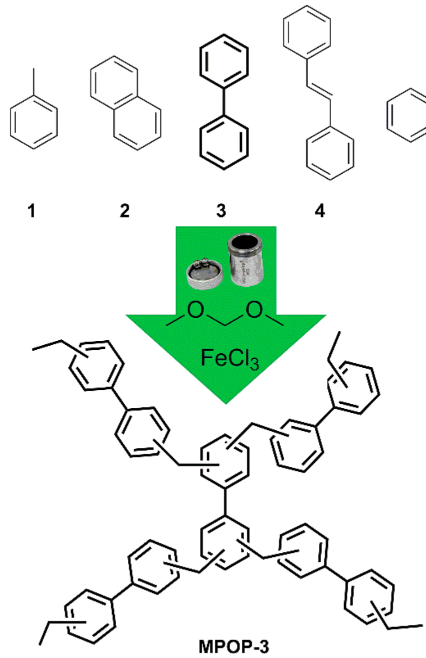

Scheme 1. Schematic representation of mechano-synthesis of MPOP-1 to -5 from monomer 1 to 5, respectively; only the structure of MPOP-3 was illustrated.

Gas Adsorption

A Micromeritics ASAP 2020 Plus surface area/pore size analyzer was used to measure nitrogen and carbon dioxide physisorption isotherms. *ca.* 100 mg of sample was used for each measurement. High-purity gases were used. Pore size distribution was calculated from the nitrogen adsorption isotherm based on DFT model in the Micromeritics ASAP 2020 plus software package.

Tandem Mass Spectrometry (MS/MS) Method Development

Tandem mass spectrometry (MS/MS) method was developed on a mass spectrometer (Ionics 3Q 320, Perkin Elmer, USA) in a multiple reaction monitoring (MRM) mode. The analysis was performed with an electrospray ionization source set in a positive mode. An ion-spray voltage of +5.5 kV was applied. The heated capillary temperature was set at 200 °C considering the relatively low boiling points of PNP and PNC. Drying gas and nebulizer gas were set at 120 and 350 µL/min, respectively. To determine the MS transitions, two diluted methanol solutions with 0.1% formic acid, one for the analyte (PNP) and the other for internal standard (PNC), were infused into the mass spectrometer by using a syringe pump, respectively. For analyte, the molecular ion was detected at m/z 140.1, the most intense product ions resulting from fragmentation were identified as m/z 123.1, m/z 93.2, and m/z 65.3. For internal standard, the molecular ion was detected at m/z 155.8, the most intense product ions resulting from fragmentation were identified as m/z 139.2, m/z 109.2, and m/z 81.2. These values are in good agreement with NIST (National Institute of Standards and Technology) Chemistry Webbook. Furthermore, mass spectrometry parameters including entrance voltage, collision energy, and collision cell lens 2 were fine-tuned and listed in **Table S3** in Electronic Supplementary Information.

Liquid Chromatography (LC) Method Development

Liquid chromatography (LC) method was developed on a UPLC system (ultrahigh pressure liquid chromatography, Altus A-30, Perkin Elmer, USA). Analyte separation was carried out on a Brownlee SPP C18 column (50 × 3.0 mm, 2.7 µm) maintained at 30 °C. Elution was in gradient mode with a mobile phase composed of a mixture of acetonitrile and water containing 0.1% formic acid pumped at 0.5 mL/min. The total run time for the analysis was 5 min. A high rate of elution was necessary to achieve a short analytical run. The detail of gradient elution setup was in **Table S4** in Electronic Supplementary Information.

A diluted aqueous solution containing both PNP (analyte) and PNC (internal Standard) were subjected to auto sampling for the developing of the LC method. The retention of PNP and PNC were 1.64 and 3.05 min with tuned gradient elution, respectively. The total ion chromatogram with a good separation of PNP and PNC as well as high intensity for both was shown in **Figure S13** in Electronic Supplementary Information.

LC-MS/MS Method Development

PNP concentrations were measured on the UPLC system coupled with the mass spectrometer under conditions as described above. First, a stock solution of PNP (1 mg/mL, 1000 ppm) and a stock solution of PNC (0.1 mg/mL, 100 ppm) were prepared in deionized water. Both stock solutions were stored at 20 °C and wrapped in aluminum foil to prevent photodegradation. Then, working solutions of PNP for calibration were prepared at seven different concentrations (2, 5, 10, 20, 50, 100, 200 ppm), and PNC was added to each solution at a final concentration of 50 ppm. For example, the 200-ppm working solution was prepared by mixing 0.2 mL of PNP stock solution, 0.5 mL of PNC stock solution and 0.3 mL of water; the 100-ppm working solution was prepared by mixing 0.1 mL of PNP stock solution, 0.5 mL of PNC solution, and 0.4 mL of water; and so on.

Calibration Curve

All seven working solutions were run seven times to eliminate any experimental error. The PNP concentration was plotted against the PNP/PNC peak area ratio. All seven calibration curves showed good linearity throughout the used range of concentration. A linear regression line was fitted to the experimental data as shown in **Figure 1** and its correlation coefficient (R^2) was calculated to be 0.99854.

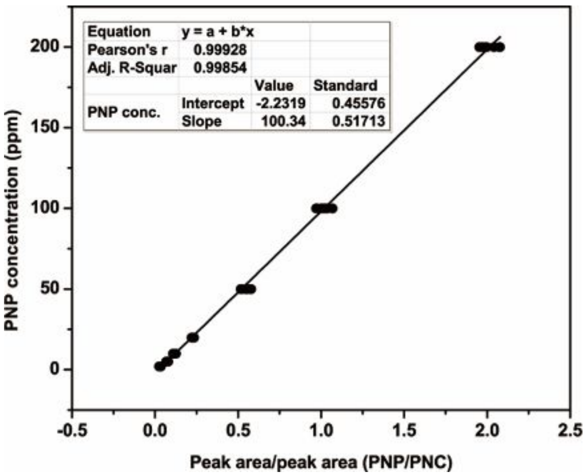

Figure 1. LC-MS/MS calibration curve of PNP with PNC as an internal standard.

Adsorption of PNP with MPOP-1 and MPOP-3

To a 500-ppm aqueous solution of PNP (100 mL), added dried MPOP-1 or MPOP-3 (200 mg), it was shaken for 30 s and then left to stand still. For MPOP-1, a 0.5 mL of above solution was taken at intervals of 5, 10, 30, 60, 180, 360 min, 1 d, 2 d, and 5 d, respectively; For MPOP-3, a 0.5 mL of solution was taken at intervals of 5, 10, 30, 120, 240, 360 min, 1 d, 2 d, and 5 d, respectively. Each of these solutions was added 0.5 mL of stock solution of PNC (100 ppm), which made the PNC as an internal standard at a final concentration of 50 ppm in all the solutions. Before mounted on autosampler in UPLC for analysis, all the solutions were filtered with 0.2 µm polypropylene syringe filters.

Results and discussion

To investigate the porosities of the MPOPs, nitrogen adsorption-desorption measurements at 77 K up to 1 bar pressure were performed. Before analysis, these polymers were degassed under dynamic vacuum at 80 °C for 8 h. The nitrogen sorption isotherms and corresponding pore size distribution curves are shown in **Figure 2**. Brunauer-Emmett-Teller (BET) surface area calculation was carried out by using ASAP 2020 plus software. Isotherm points chosen to calculate the BET surface area were subject to the three consistency criteria detailed by Walton and Snurr.[13] First, the pressure range selected has values of V(Po − P) increasing with P/Po. Second, the point used to calculate the BET surface area is linear with an upward slope. Third, the line has a positive y-intercept (**Figure S1** to **S5**). The calculated BET surface areas for MPOP-1 to -5 were 374, 71, 556, 375, and 129 m^2/g, respectively.

MPOP-2, the one from naphthalene, exhibited the lowest surface area probably because of the planarity of naphthalene molecule, which is clearly favoured for a two-dimensional extension, not three-dimensional hyper-cross linking. The other monomers, on the other hand, wherein individual phenyl rings are mostly free to rotate and adopt an orthogonal orientation to the rest of the molecule, are more likely extending into hyper-crosslinked three-dimensional networks. Among them, MPOP-5, the one from tetraphenylethylene, showed a low surface area probably because of the relative rigidity of the molecule itself imposed by the central double bond. MPOP-3, the one from biphenyl, showed the highest surface area, probably due to its preferred conformation where two phenyl rings are perpendicular to each other, such a geometry is favoured and translated into a three-dimensional polymer.[1e] These values, however, are somewhat lower than those made with traditional polymerization reactions in solutions (the reported surface areas were usually in the range of 500 to 1200 m^2/g),[5c, 14] nevertheless, our approach is greener and sustainable by avoiding the large quantity of 1,2-dichloroethane or other chlorinated solvents used in conventional Friedel-Crafts reactions, and our continued efforts to improve the surface area by optimizing the reaction conditions is underway.

The DFT method was used to calculate the pore size distribution, and most of the observed pores were in the microporous region, which is usually the case in hyper-crosslinking (1 to 2 nm, **Figure 2**). Some mesopores were also observed, and this could possibly be attributed to the voids between aggregates of nano-sized polymeric particles, which is rather common in porous organic polymers.[15] The nitrogen sorption isotherms showed that desorption branch does not coincide with the adsorption branch. This may be due to the existence of extremely narrow micropores that kinetically restrict the exit of adsorbed nitrogen molecules from the interior during pressure releasing the desorption process.[16]

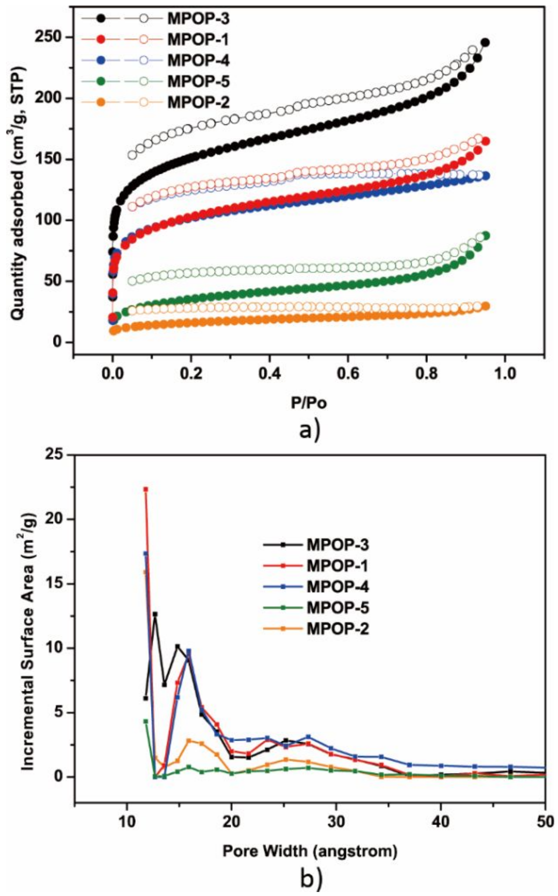

Figure 2. a) Nitrogen adsorption (closed)/desorption (open) isotherms of MPOP-1 to -5 at 77 K; b) Pore size distribution of MPOP-1 to -5 calculated from their individual nitrogen adsorption curve.

To confirm that, we probed MPOP-3 with CO_2 at higher temperatures (Figure S19). no large hysteresis loops in the adsorption/desorption isotherms were observed, and the tiny hysteresis loop was becoming even smaller as temperature increased from 273 K to 295 K to 313 K, which are consistent with the literature.[17]

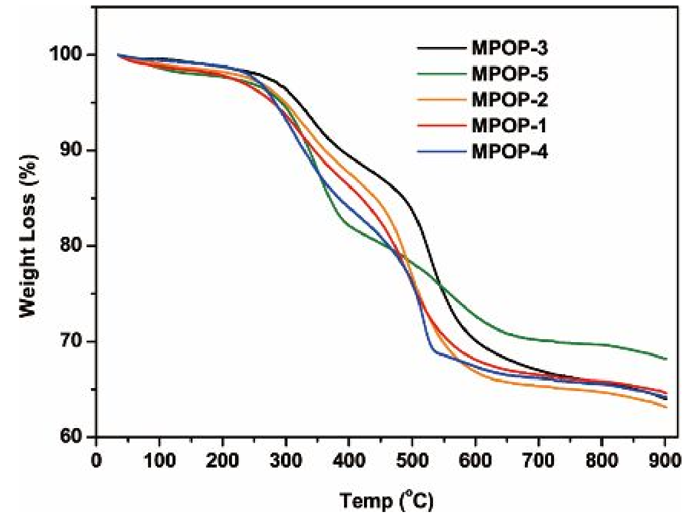

Figure 3. Thermogravimetric analysis of MPOP-1 to -5 under a nitrogen atmosphere.

The obtained MPOPs were characterized by Fourier transform infrared spectroscopy (FT-IR). As shown in **Figure S11**, peaks near 3000 cm^{-1} can be attributed to the bending and stretching vibrations of C-H on aromatic rings and newly formed methylene groups. The C-O stretching vibrations near 1250 cm^{-1} can be assigned to the methoxyl groups formed during the Friedel-Crafts reactions, indicating the incompletion of the polymerization. The chemical structures of MPOPs were further identified by solid-state ^{13}C NMR (**Figure S20** to **S24**). The intensified peaks near 140 ppm represent the aromatic and alkenyl carbons; the peaks are appearing near 40 ppm are ascribed to the carbons of methylene linkers. For MPOP-1, the strong peak near 16 ppm is due to the benzylic carbon originating from the starting material toluene.

Thermogravimetric analyses of the MPOP materials were carried out with a heating temperature up to 900 °C at a ramping rate of 5 °C/min under a continuous nitrogen atmosphere (**Figure 3**). All the MPOPs showed no obvious weight loss before 200 °C and retained more than 60% of their mass even at 900 °C, indicating a good thermal stability, which is consistent with the reports for other hyper-crosslinked materials.[5c, 18] Compared to PAF-1 (520 °C)[1a] or PPN-4 (450 °C)[1l], in which the unusual stability are derived from their rigid aromatic ring structures, our MPOP materials have relatively lower thermal stability, we suspect that the intrinsical methylene crossing between aromatic rings make the framework relatively flexible, therefore, more susceptible to collapsing during the heating process.

SEM images revealed that MPOP particles were spherical in shape with dimensions in submicrometer range, which is typical for highly cross-linked polymers, likely in aggregated forms (**Figure S6** to **S10**). Wavelength-Dispersive X-Ray Spectroscopy (WDS) analysis was carried out to measure the contents of residue iron and chlorine in these MPOP materials (**Table S2**). The weight percentage of Fe varied from 0.178% to 0.799%, even after refluxing the MPOPs in 3.0 M aqueous HCl solutions overnight twice, indicating some of the iron species were trapped inside the MPOP materials, which is usually the case for amorphous porous polymers. However, considering its high molecular weight, the iron contents are much less significant in terms of molar percentage. The weight percentage of Cl varied from 0.119% to 0.410% for MPOP-1, MPOP-2, MPOP-3, and MPOP-5, interestingly, the Cl% value is much higher for MPOP-4 (1.078%), which could be attributed to a certain degree of HCl (by-product of Friedel-Crafts reaction) addition onto the double bond in the skeletal network since stilbene the monomer contains a di-substituted double bond, which is relatively reactive. It was not the case for MPOP-5, however, because the double bond in tetraphenylethylene is tetra-substituted and rather inert.

Nitrophenols are widely used in petrochemical synthesis, including paints, plastics, rubber, pulp, pesticides and dyes production.[19] p-Nitrophenol (PNP), in particular, has an intensive toxic effect on methemoglobin formation, potentially causing cyanosis, confusion, and unconsciousness. It has been listed as a priority pollutant by the U. S. Environmental Protection Agency.[20] The presence of nitrophenols in industrial wastewater has aroused great concerns in recent years due to the increase in wastewater discharge and the toxicity of nitrophenols to the receiving bodies.[21] For years, to minimize nitrophenol pollution from wastewater, the methods of photo-degradation,[22] adsorption,[23] and chemical oxidation,[24] etc, have been developed. Among them, physical adsorption is one of the most promising techniques due to the advantages such as low cost, simple operation, and reuse.[21b]

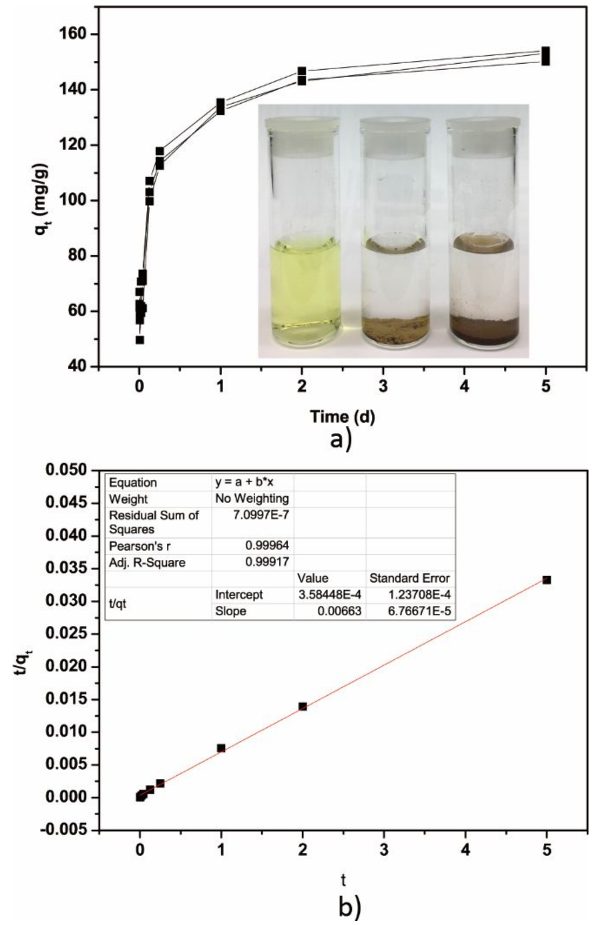

Figure 4. a) PNP adsorption curves for MPOP-3, inset is the picture of PNP in aqueous solutions with and without MPOPs; b) Pseudo-second-order plot for PNP adsorption on MPOP-3.

The frameworks of these MPOPs are predominantly aromatic structures, which might implicate strong interactions with organic pollutants bearing aromatic rings. Therefore, the two with higher surface areas (MPOP-1 and MPOP-3) were selected to study their performances in the removal of PNP from water. Indeed, the characteristic yellow colour of PNP anions in aqueous solutions under neutral conditions ($\lambda_{ab}^{max} \approx$ 400 nm) quickly disappeared when MPOP-1 or MPOP-3 was added (**Figure 4a inset**). To quantitate their adsorptive capacity, a UPLC system (Altus A-30, Perkin Elmer, USA) coupled with a mass spectrometer (Ionics 3Q 320, Perkin Elmer, USA) was employed and a calibration curve was first built for PNP with PNC as an internal standard and was used later on for calculating the analyte concentrations (**Figure 1**). For each MPOP, seven sample solutions were collected at different time intervals and analysed with LC-MS/MS method as described in Experimental section. All the tests were performed in triplicates. The detailed adsorption data and calculated concentrations were in **Table S6** and **S7**. The maximum adsorption of MPOP-1 and MPOP-3 for PNP were estimated to be 133.10 mg/g (**Figure S14**) and 152.51 mg/g (**Figure 4a**), respectively. After refluxed in ethanol twice, filtered, and dried, the recovered MPOP-3 was checked its N_2 adsorption at 77 K. We found that its porosity was about the same as the as-synthesized one, indicating the integrity of the network during the PNP adsorption (**Figure S25**).

To analyse the adsorption kinetics of MPOPs, the adsorption data in **Figure S14** (for MPOP-1) and **Figure 4a** (for MPOP-3) were fitted with pseudo-first-order and pseudo-second-order kinetic models, respectively. **Table S5** summarized the adsorption kinetic parameters of PNP on these two tested sorbents. Comparing with the correlation coefficients (R^2) of the Pseudo-first-order and Pseudo-second-order, it can be easily concluded that the Pseudo-second-order kinetic model fits the adsorption process for both tested sorbents better than Pseudo-first-order. The fitting lines of Pseudo-second-order were perfectly plotted in **Figure S15** (for MPOP-1) and **Figure 4b** (for MPOP-3). This suggests that the rate of adsorption of PNP on MPOPs is not simply diffusion controlled, but rather depends on the availability of adsorption sites, in this case, aromatic rings in the framework, therefore, the maximum PNP adsorption capacity is correlated to surface area, with MPOP-3 having the higher PNP adsorption capacity. Compared to other porous materials tested for the removal of PNP from water, our materials exhibit moderate adsorption capacities (**Table 1**). Considering the cost-effective synthesis and easiness to scale-up, MPOPs are very promising in terms of water treatment applications in this line, not to mention the fact that adsorption capacity is proportional to the surface area in this type of materials, which suggests the possibility of further improving the adsorption capacity through optimization of reaction conditions.

Table 1. Maximum adsorption capacities of PNP for some selected sorbents at room temperature.

Sorbents	Surface area (m^2/g)	q_{max} (mg/g)	Ref.
NiAl-LDH	108.7	77.7	19b
Polymer1	38.45	101.6	25
MPOP-1	374	133.10	This work
MPOP-3	556	152.51	This work
NH_2-MIL101(Al)	1942	195.52	26
PAC-NUT	679	234.3	27

Conclusions

In this work, we successfully demonstrated a mechano-synthesis of porous organic polymers *via* a ball-milling procedure. Several readily available benzene derivations were selected to be polymerized through a Friedel-Crafts reaction with anhydrous $FeCl_3$ as Lewis acid and formaldehyde dimethyl acetal as a crosslinker. All the polymers are not soluble in common organic solvents. The calculated BET surface area can reach over 500 m^2/g with biphenyl as the monomer. One of the advantages of applying ball-milling in targeted polymer synthesis is avoiding large quantity of hazardous organic solvents which are commonly used in traditional Friedel-Crafts reactions. Considering the aromatic skeletal network and the hydrophobic nature of these mechano-synthesized porous organic polymers (MPOP), their performances in p-nitrophenol (PNP) adsorption from water were investigated. The quantification was carried out on an LC-MS/MS system with 4-nitrocatechol (PNC) as an internal standard. MPOP-3 shows a maximum PNP absorption capacity as high as 152.51 mg/g. The adsorption isotherms can be well delineated with a pseudo-second-order equation, indicating the availability of strong adsorption sites in both MPOPs for interacting with PNP.

Conflicts of interest

The authors declare no conflicts of interest.

Acknowledgements

This work was supported by Jinan University (W. Lu), Washington State University (L. Hao and Q. Zhang), and Fayetteville State University (W. Lu and Z. Luo). Electron Microprobe Facility at Fayetteville State University was funded by the U.S. Department of Defense grants W911NF-09-1-0011 and W911NF-15-1-0566.

References

1. (a) T. Ben, H. Ren, S. Ma, D. Cao, J. Lan, X. Jing, W. Wang, J. Xu, F. Deng, J. M. Simmons, S. Qiu and G. Zhu, *Angewandte Chemie International Edition*, 2009, **48**, 9457; (b) S. Das, P. Heasman, T. Ben and S. Qiu, *Chemical Reviews*, 2017, **117**, 1515; (c) R. Dawson, A. I. Cooper and D. J. Adams, *Progress in Polymer Science*, 2012, **37**, 530; (d) P. Kuhn, A. Forget, D. Su, A. Thomas and M. Antonietti, *Journal of the American Chemical Society*, 2008, **130**, 13333; (e) W. Lu, Z. Wei, D. Yuan, J. Tian, S. Fordham and H.-C. Zhou, *Chemistry of Materials*, 2014, **26**, 4589; (f) W. Lu, D. Yuan, D. Zhao, C. I. Schilling, O. Plietzsch, T. Muller, S. Bräse, J. Guenther, J. Blümel, R. Krishna, Z. Li and H.-C. Zhou, *Chemistry of Materials*, 2010, **22**, 5964; (g) L. Tan and B. Tan, *Chemical Society Reviews*, 2017, **46**, 3322; (h) D. Wu, F. Xu, B. Sun, R. Fu, H. He and K. Matyjaszewski, *Chemical Reviews*, 2012, **112**, 3959; (i) Z. Xiang and D. Cao, *Journal of Materials Chemistry A*, 2013, **1**, 2691; (j) Y. Xu, S. Jin, H. Xu, A. Nagai and D. Jiang, *Chemical Society Reviews*, 2013, **42**, 8012; (k) X.-Y. Yang, L.-H. Chen, Y. Li, J. C. Rooke, C. Sanchez and B.-L. Su, *Chemical Society Reviews*, 2017, **46**, 481; (l) D. Yuan, W. Lu, D. Zhao and H.-C. Zhou, *Advanced Materials*, 2011, **23**, 3723.
2. (a) H.-C. Zhou, J. R. Long and O. M. Yaghi, *Chemical Reviews*, 2012, **112**, 673; (b) J. R. Long and O. M. Yaghi, *Chemical Society Reviews*, 2009, **38**, 1213; (c) H.-C. Zhou and S. Kitagawa, *Chemical Society Reviews*, 2014, **43**, 5415; (d) K. Adil, Y. Belmabkhout, R. S. Pillai, A. Cadiau, P. M. Bhatt, A. H. Assen, G. Maurin and M. Eddaoudi, *Chemical Society Reviews*, 2017, **46**, 3402.

3. (a) W. Lu, J. P. Sculley, D. Yuan, R. Krishna, Z. Wei and H.-C. Zhou, *Angewandte Chemie International Edition*, 2012, **51**, 7480; (b) W. Lu, D. Yuan, J. Sculley, D. Zhao, R. Krishna and H.-C. Zhou, *Journal of the American Chemical Society*, 2011, **133**, 18126.
4. (a) S. Xu, Y. Luo and B. Tan, *Macromolecular Rapid Communications*, 2013, **34**, 471; (b) B. Li, R. Gong, W. Wang, X. Huang, W. Zhang, H. Li, C. Hu and B. Tan, *Macromolecules*, 2011, **44**, 2410; (c) R. Dawson, T. Ratvijitvech, M. Corker, A. Laybourn, Y. Z. Khimyak, A. I. Cooper and D. J. Adams, *Polymer Chemistry*, 2012, **3**, 2034.
5. (a) Y. Luo, B. Li, W. Wang, K. Wu and B. Tan, *Advanced Materials*, 2012, **24**, 5703; (b) X. Jing, D. Zou, P. Cui, H. Ren and G. Zhu, *Journal of Materials Chemistry A*, 2013, **1**, 13926; (c) X. Zhu, S. M. Mahurin, S.-H. An, C.-L. Do-Thanh, C. Tian, Y. Li, L. W. Gill, E. W. Hagaman, Z. Bian, J.-H. Zhou, J. Hu, H. Liu and S. Dai, *Chemical Communications*, 2014, **50**, 7933; (d) N. Chaoui, M. Trunk, R. Dawson, J. Schmidt and A. Thomas, *Chemical Society Reviews*, 2017, **46**, 3302; (e) R. Dawson and A. Trewin, in *Porous Polymers: Design, Synthesis and Applications*, The Royal Society of Chemistry, 2016, pp. 155; (f) Z. Kahveci, A. K. Sekizkardes, R. K. Arvapally, L. Wilder and H. M. El-Kaderi, *Polymer Chemistry*, 2017, **8**, 2509; (g) M. G. Rabbani, T. Islamoglu and H. M. El-Kaderi, *Journal of Materials Chemistry A*, 2017, **5**, 258; (h) B. Ashourirad, P. Arab, T. Islamoglu, K. A. Cychosz, M. Thommes and H. M. El-Kaderi, *Journal of Materials Chemistry A*, 2016, **4**, 14693.
6. (a) S. Bhunia, B. Banerjee and A. Bhaumik, *Chemical Communications*, 2015, **51**, 5020; (b) S. Gu, J. He, Y. Zhu, Z. Wang, D. Chen, G. Yu, C. Pan, J. Guan and K. Tao, *ACS Applied Materials & Interfaces*, 2016, **8**, 18383; (c) X. Zhu, S. Ding, C. W. Abney, K. L. Browning, R. L. Sacci, G. M. Veith, C. Tian and S. Dai, *Chemical Communications*, 2017, **53**, 7645.
7. N. B. McKeown and P. M. Budd, *Macromolecules*, 2010, **43**, 5163.
8. K. J. Msayib and N. B. McKeown, *Journal of Materials Chemistry A*, 2016, **4**, 10110.
9. (a) E. Troschke, S. Grätz, T. Lübken and L. Borchardt, *Angewandte Chemie International Edition*, 2017, **56**, 6859; (b) X. Zhu, C. Tian, T. Jin, K. L. Browning, R. L. Sacci, G. M. Veith and S. Dai, *ACS Macro Letters*, 2017, **6**, 1056.
10. J.-L. Do and T. Friščić, *ACS Central Science*, 2017, **3**, 13.
11. in *Ball Milling Towards Green Synthesis: Applications, Projects, Challenges*, The Royal Society of Chemistry, 2015, pp. P001.
12. (a) M. Gros, M. Petrović and D. Barceló, *Talanta*, 2006, **70**, 678; (b) Y.-T. Wong, W.-K. Law, S. S.-L. Lai, S.-P. Wong, K.-C. Lau and C. Ho, *Analytical Methods*, 2018, **10**, 3514.
13. K. S. Walton and R. Q. Snurr, *Journal of the American Chemical Society*, 2007, **129**, 8552.
14. (a) Y. Luo, S. Zhang, Y. Ma, W. Wang and B. Tan, *Polymer Chemistry*, 2013, **4**, 1126; (b) R. T. Woodward, L. A. Stevens, R. Dawson, M. Vijayaraghavan, T. Hasell, I. P. Silverwood, A. V. Ewing, T. Ratvijitvech, J. D. Exley, S. Y. Chong, F. Blanc, D. J. Adams, S. G. Kazarian, C. E. Snape, T. C. Drage and A. I. Cooper, *Journal of the American Chemical Society*, 2014, **136**, 9028; (c) Y. Yang, C. Y. Chuah, H. Gong and T.-H. Bae, *Journal of CO2 Utilization*, 2017, **19**, 214.
15. E. Stockel, X. Wu, A. Trewin, C. D. Wood, R. Clowes, N. L. Campbell, J. T. A. Jones, Y. Z. Khimyak, D. J. Adams and A. I. Cooper, *Chemical Communications*, 2009, 212.
16. S. Xiong, X. Fu, L. Xiang, G. Yu, J. Guan, Z. Wang, Y. Du, X. Xiong and C. Pan, *Polymer Chemistry*, 2014, **5**, 3424.
17. P. I. Ravikovitch, A. Vishnyakov, R. Russo and A. V. Neimark, *Langmuir*, 2000, **16**, 2311.
18. H. Li, B. Meng, S.-H. Chai, H. Liu and S. Dai, *Chemical Science*, 2016, **7**, 905.
19. (a) V. N. Yarlagadda, R. Kadali, N. Sharma, R. Sekar and V. Vayalam Purath, *Applied Biochemistry and Biotechnology*, 2012, **166**, 1225; (b) Y. Sun, J. Zhou, W. Cai, R. Zhao and J. Yuan, *Applied Surface Science*, 2015, **349**, 897.
20. V. Uberoi and S. K. Bhattacharya, *Water Environment Research*, 1997, **69**, 146.
21. (a) G. Xue, M. Gao, Z. Gu, Z. Luo and Z. Hu, *Chemical Engineering Journal*, 2013, **218**, 223; (b) Z. Wu, X. Yuan, H. Zhong, H. Wang, G. Zeng, X. Chen, H. Wang, L. zhang and J. Shao, *Scientific Reports*, 2016, **6**, 25638.
22. Y. Tuo, G. Liu, B. Dong, J. Zhou, A. Wang, J. Wang, R. Jin, H. Lv, Z. Dou and W. Huang, *Scientific Reports*, 2015, **5**, 13515.
23. Q. Jing, Z. Yi, D. Lin, L. Zhu and K. Yang, *Water Research*, 2013, **47**, 4006.
24. R. S. Ribeiro, A. M. T. Silva, J. L. Figueiredo, J. L. Faria and H. T. Gomes, *Applied Catalysis B: Environmental*, 2013, **140-141**, 356.
25. Q. Zhang, C. Peter Okoli, L. Wang and T. Liang, *Desalination and Water Treatment*, 2015, **55**, 1575.
26. B. Liu, F. Yang, Y. Zou and Y. Peng, *Journal of Chemical & Engineering Data*, 2014, **59**, 1476.
27. S. Álvarez-Torrellas, M. Martin-Martinez, H. T. Gomes, G. Ovejero and J. García, *Applied Surface Science*, 2017, **414**, 424.

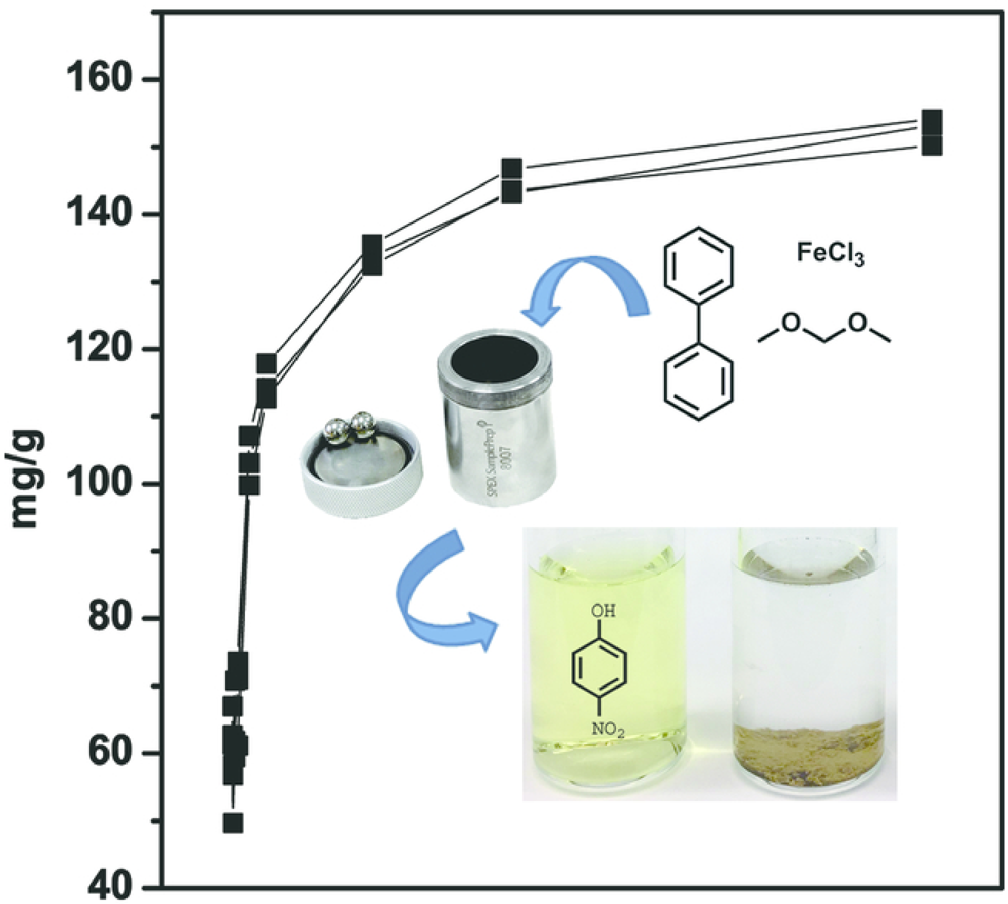

54x49mm (300 x 300 DPI)